Journal of Metals, Materials and Minerals, 36(3), e2636, 2026

Magnetocaloric effect of GdTbDyErPr rare-earth high-entropy alloy

Yu LIU[1,2], Lei GAO[3], Jun PENG[1,*], and Haitao GUO[2]

[1] *School of Rare Earth Industry, Inner Mongolia University of Science and Technology, Baotou, China*
[2] *Baotou Rewin Rare Earth Metal Materials Co.,Ltd., Baotou, China*
[3] *National Key Laboratory of Baiyunobo Rare Earth Resource Research and Comprehensive Utilization, Baotou Research Institute of Rare Earths, Baotou, China*

***Corresponding author e-mail**: pengjun75@163.com

Received date:
28 January 2026
Revised date:
22 February 2026
Accepted date:
27 February 2026

Keywords:
Rare-earth high-entropy alloy;
HCP structure;
Magnetic properties;
Magnetocaloric effect

Abstract

In this study, a GdTbDyErPr rare-earth high-entropy alloy (RE HEA) was successfully synthesized and its magnetic properties and magnetocaloric effect (MCE) were systematically investigated. The results indicate that the as-cast GdTbDyErPr RE HEA exhibits a single-phase hexagonal close-packed (HCP) structure with lattice parameters of a = 3.609 Å and c = 5.734 Å. Based on large parameter Ω, high mixing entropy (ΔSmix), and small parameters δ and εi, it can be inferred that the GdTbDyErPr alloy forms a disordered solid solution. The GdTbDyErPr RE HEA undergoes a first-order magnetic transition near about 143 K. The parameters $|\Delta S_M^{pk}|$, RC, and RCP are determined to be 6.8 J·kg^{-1}K^{-1}, 352 J·kg^{-1} and 462 J·kg^{-1} for GdTbDyErPr RE HEA under 0 T to 5 T. The facile synthesizability and remarkable MCE of the GdTbDyErPr RE HEA position it as a promising candidate for magnetic cooling technology

1. Introduction

Compared to gas-compression refrigeration, magnetic refrigeration has attracted extensive attention due to its environmental friendliness, high energy efficiency and so on [1–5]. Magnetic refrigeration is a cooling method based on the magnetocaloric effect (MCE), which is a thermodynamic phenomenon observed in magnetic materials [6–12]. This effect manifests as the absorption or release of heat when the material is exposed to a time-varying magnetic field [13–17]. The MCE can be characterized by the magnetic-field-induced entropy change (ΔSm), which originates from the reorientation of atomic magnetic moments under an applied external magnetic field [18–20]. Research on magnetic refrigeration technology primarily focuses on three aspects: magnetic refrigerants, systems capable of generating high-intensity magnetic fields with rapid variation, and the design of refrigeration devices [21–24]. Current investigations into magnetic refrigerants are mainly concentrated on conventional alloys (e.g., Gd, $Gd_5(Si,Ge)_4$, $La(Fe,Si)_{13}$, MnFePAs, and Heusler alloys), perovskites (e.g., $LaMnO_3$), and composite materials (e.g., LaFeSi/PrCo) [2]. Among them, certain materials such as Gd and its derivatives, $Gd_5(Si,Ge)_4$-based, and $La(Fe,Si)_{13}$-based alloys have already found applications in magnetic refrigerators [25]. However, their practical implementation has also revealed several challenges, for instance, $La(Fe,Si)_{13}$-based alloy with poor mechanical properties may undergo pulverization after prolonged service, ultimately causing them to fail.

As a novel alloy design strategy, high-entropy alloys (HEAs) are a class of novel materials composed of five or more principal elements, each with an equal or near-equal atomic percentage (at%) [26–28]. High-entropy alloys (HEAs) are regarded as a transformative innovation in the design and development of advanced materials. Their outstanding properties, including mechanical performance, phase stability, wear resistance, and corrosion resistance, significantly surpass those of conventional alloys [29–31]. HEAs have attracted increasing research interest in both fundamental science and engineering applications. While the rapid advancement of HEA research has spurred the development of two material generations (from first-generation equiatomic single-phase to the focus of recent years on second-generation multiphase and non-equiatomic materials), investigative efforts have been largely confined to structural applications [28,29]. Studies demonstrate that the multi-principal-element mixture in HEAs produces key phenomena-including the high-entropy effect, sluggish diffusion, lattice distortion, and cocktail effect-that underpin the theoretical basis for their outstanding magnetic and magnetocaloric properties [27–28]. Numerous studies have shown that alloys containing rare-earth (RE) elements typically exhibit a superior MCE compared to their rare-earth-free counterparts, due to the large intrinsic magnetic moments of the RE elements [1,2,32]. Therefore, applying the HEA concept to develop high MCE RE-based materials is both scientifically intriguing and technologically crucial. Although previous studies have primarily focused on the MCE of RE-based high-entropy metallic glasses, a critical limitation remains their inherently poor glass-forming ability, despite their promising properties [33–35]. In response to this challenge, the magnetic properties and MCE of as-cast GdTbDyErPr HEA with crystallographic structure were systematically investigated in this study.

2. Experimental

The alloy ingot with a nominal composition of GdTbDyErPr was prepared by conventional arc-melting under a high-purity argon atmosphere. The raw materials were metallic Gd, Tb, Dy, Er, and Pr with purities better than 99.9 wt%. To ensure chemical homogeneity, the ingots were remelted at least four times. The phase structure of the alloy was examined by X-ray diffraction (XRD; Cu Kα radiation) with a 2θ range from 10° to 80°. Microstructural characterization and chemical analysis were performed using scanning electron microscopy (SEM) equipped with energy-dispersive X-ray spectroscopy (EDS). Magnetic properties were measured using a comprehensive physical property measurement system (PPMS, Quantum Design). The thermo-magnetic curves under zero-field-cooling (ZFC) and field-cooling (FC) conditions were measured as follows: for the ZFC curve (M_{ZFC}-T curve), the sample was first cooled to 5 K in zero magnetic field. A magnetic field of 0.05 T was then applied, and the magnetization was recorded while heating to 300 K at a constant rate of 5 K·min^{-1}. For the FC curve (M_{FC}-T curve), the sample was cooled from 300 K to 5 K under an applied field of 0.05 T, after which the magnetization was measured during subsequent heating to 300 K under the same field, also at a heating rate of 5 K·min^{-1}. Isothermal magnetization curves (M-$\mu_0 H$ curve) were measured at various temperatures by applying magnetic fields up to 5 T. Both the ascending (increasing field) and descending (decreasing field) branches were recorded to assess magnetic hysteresis.

3. Results and discussion

Figure 1 shows the XRD pattern of the GdTbDyErPr alloy. All diffraction peaks can be indexed to a hexagonal close-packed (HCP) structure with space group P63/mmc, indicating a single-phase structure. In contrast, Rietveld refinement of the XRD pattern using Maud refined software yielded experimental values of a = 3.609 Å and c = 5.734 Å. Figure 2 shows the scanning electron microscopy (SEM) image of the GdTbDyErPr alloy. The absence of noticeable contrast or secondary phases in the microstructure further confirms its single-phase nature, consistent with the XRD results. The corresponding energy-dispersive X-ray spectroscopy (EDS) elemental maps in Figure 3(a) reveal a homogeneous elemental distribution of Gd, Tb, Dy, Er, and Pr without detectable segregation. Moreover, the measured chemical compositions of these elements are close to the nominal stoichiometry (Figure 3(b)). These results collectively confirm the successful synthesis of a homogeneous, single-phase GdTbDyErPr alloy with a uniform elemental distribution.

To evaluate the role of mixing entropy in stabilizing the phase of the GdTbDyErPr HEA, the parameter Ω was calculated [36].

$$\Omega = \frac{T_m \Delta S_{mix}}{|\Delta H_{mix}|} \quad (1)$$

where Tm, ΔSmix, and ΔHmix represent the average melting temperature, mixing entropy, and mixing enthalpy, respectively.

$$T_m = \sum_{i=1}^{n} c_i (T_m)_i \quad (2)$$

$$\Delta S_{mix} = -R \sum_{i=1}^{n} c_i \ln(c_i) \quad (3)$$

$$\Delta H_{mix} = \sum_{i=1, i\neq j}^{n} \Omega_{ij} c_i c_j = 4 \sum_{i=1, i\neq j}^{n} \Delta H_{ij}^{mix} c_i c_j \quad (4)$$

In this expression, $(T_m)_i$ represents the melting point of the i-th element, R is the gas constant (8.314 J·K^{-1}·mol^{-1}), c_i is the molar ratio, and ΔH_{ij}^{mix} denotes the mixing enthalpy between the i-th and j-th elements. A Ω parameter greater than 1.1 indicates that the entropic contribution dominates over the enthalpic effect, thereby stabilizing the solid solution phase. For the equiatomic GdTbDyErPr HEA, the mixing entropy (ΔS_{mix}) is calculated as 13.38 J·mol^{-1}·K^{-1} (equivalent to 1.61R). After calculating, the overall mixing enthalpy (ΔH_{mix}) of the alloy is –36.48 kJ·mol^{-1}. Consequently, the calculated Ω parameter is large, confirming that the high mixing entropy dominates the thermo-dynamic process and favors the formation of a single solid solution phase. Despite too high negative ΔHmix between Pr and other elements exhibits, unfavorable kinetics with sluggish atomic diffusion hinders transformations in the HEA, so the simple high-temperature structure of a disordered solid solution is retained down to low temperature.

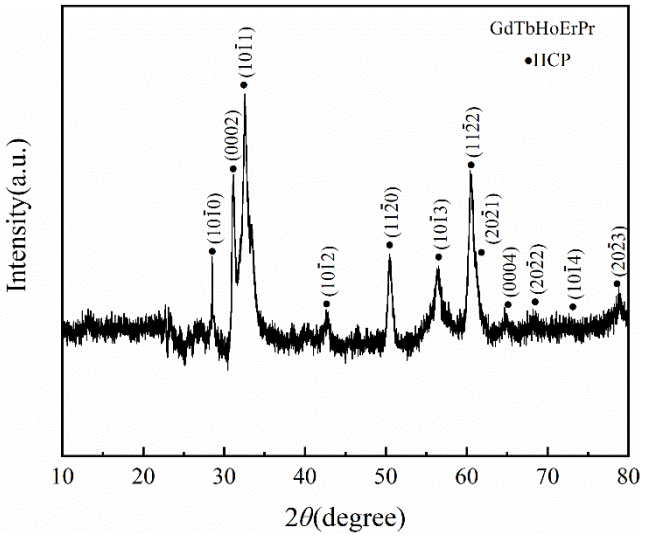

Figure 1. XRD pattern of the GdTbDyErPr RE HEA.

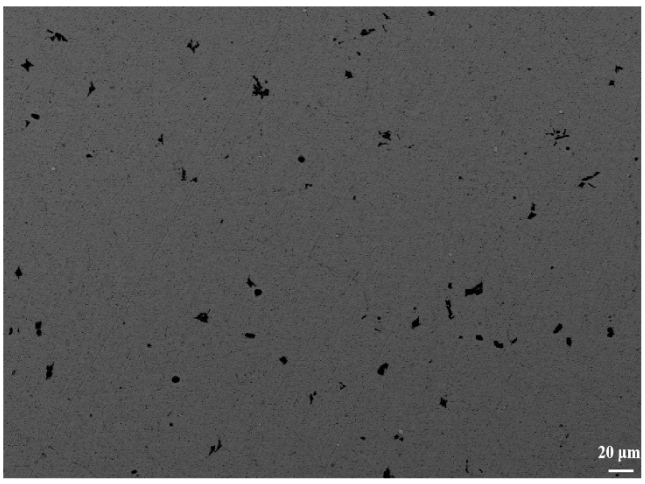

Figure 2. SEM image of the GdTbDyErPr RE HEA.

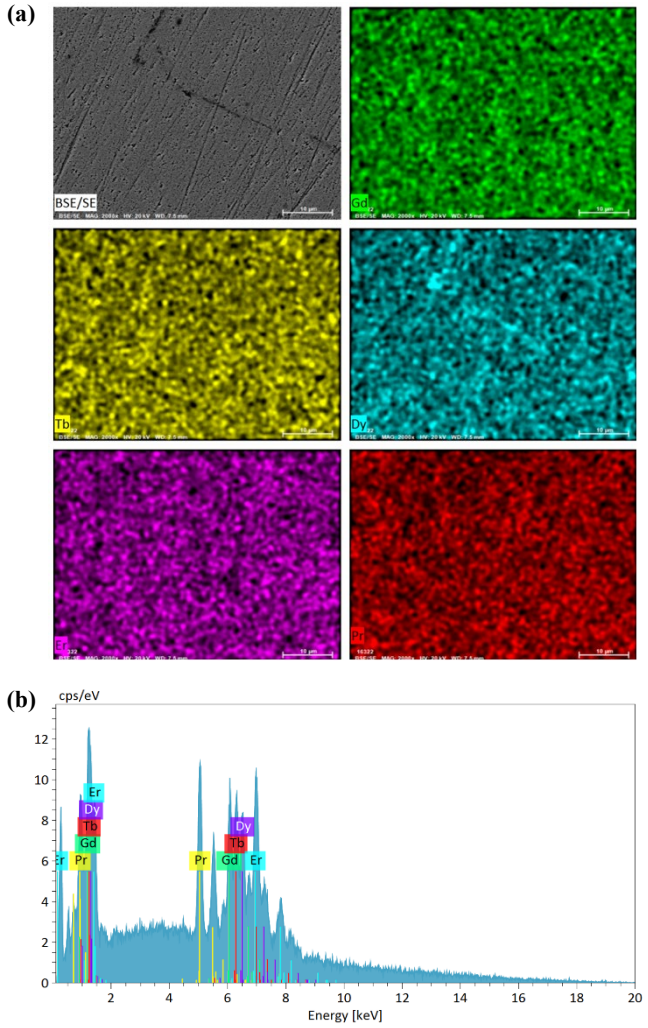

Figure 3. (a) EDS image and (b) corresponding quantitative composition of GdTbDyErPr RE HEA.

The parameter δ, defined as the atomic size difference, was proposed based on the Hume-Rothery rules to predict the structural stability and phase formation in HEAs. It is calculated using the following formula [37].

$$\delta = \sqrt{\sum_{i=1}^{n} c_i\left(1 - {}^{r_i}/_{\bar{r}}\right)^2} \tag{5}$$

In this equation, r_i represents the Goldschmidt atomic radius of the i-th element. The parameter δ quantifies the atomic size mismatch, which reflects the degree of local lattice strain and topological instability within the alloy system. A comprehensive analysis of existing data for various HEA systems suggests a critical criterion of $\delta < 4\%$ for the formation of a simple solid solution during rapid solidification. Given the similar Goldschmidt atomic radii of the constituent rare-earth elements, it is confirmed that the GdTbDyErPr HEA readily forms a single phase, as its calculated δ value approaches zero (δ = 2.23% for GdTbDyErPr RE HEA).

To provide a more accurate assessment of atomic size mismatch and lattice distortion in the present alloy, the intrinsic residual strain was also quantified via atomic size and packing efficiency metrics, in accordance with the approach established by Ye *et al*.:

$$\varepsilon_i = \frac{\sum_{j=1}^{n} \omega_{ij} c_j}{\sum_{k=1}^{n} A_{ik} c_k} - \frac{4\pi\eta}{N_i \sum_{k=1}^{n} A_{ik} c_k} \tag{6}$$

$$\omega_{ij} = 2\pi\left[1 - \frac{\sqrt{\gamma_i\left(\gamma_i + 2\gamma_j\right)}}{\gamma_i + \gamma_j}\right] \tag{7}$$

$$A_{ik} = \frac{2\pi\chi_{ik}}{\left(\chi_{ik} + 1\right)^2 \sqrt{\chi_{ik}\left(\chi_{ik} + 2\right)}} \tag{8}$$

$$\chi_{ik} = \frac{\gamma_i}{\gamma_k} \tag{9}$$

Ye et al. found that solid solutions can remain stable under a certain root mean square (R.M.S.) residual strain. Calculation results indicate that they all fall within the single solid solution region. From the perspective of strain energy, no significant lattice strain effect is observed; therefore, it is highly unlikely that the large magnetocaloric effect can be attributed to lattice distortion in GdTbDyErPr HEA.

Furthermore, other HEA formation criteria, e.g., the electronegativity difference, Δx [38] and valence electron concentration (VEC) [39][40] were also examined for the current four rare-earth alloys. These parameters can be obtained by the following equations,

$$\Delta x = \sqrt{\sum_{i=1}^{n} c_i (x - \bar{x})^2} \tag{10}$$

$$VEC = \sum_{i=1}^{n} c_i (VEC)_i \tag{11}$$

Where x_i is the Pauling electronegativity of i-th element, and $\bar{x}$ is the average electronegativity of all element. $(VEC)_i$ is the *VEC* for the i-th element. The Δx value of is calculated to be 0.098 for GdTbDyErPr. The VEC value is determined to be 3 for GdTbDyErPr RE HEA because each individual component VEC=3 for all component elements. As previously discussed, all analytical indicators confirm that the GdTbDyErPr RE HEA exhibits a single-phase structure. Owing to its extremely low δ value, a large Ω, and a small εi parameter, the GdTbDyErPr HEA can be considered an almost ideal solid solution.

Figure 4 shows the MZFC-T curve and MFC-T curve of the GdTbDyErPr HEA. Under an external magnetic field of 0.05 T, a subtle magnetic kink is observed in the MZFC-T curve. The Curie temperature (T_C) was determined to be 143 K via dM/dT-T curve, as illustrated in the inset of Figure 4. This temperature corresponds to a magnetic transition from a paramagnetic (PM) state to a long-range ferromagnetic (FM) ordered state. The experimental results show that, the significant increase in χ^{-1} near TC, confirming this follows the Curie-Weiss law. The fitting result indicates that the Curie-Weiss temperature (θ_p = 141.6 K) is close to the T_C. For GdTbDyErPr RE HEA, the theoretical effective magnetic moment (μ_{eff}^{the}) can be obtained by the following Equation (12),

$$\begin{aligned}\mu_{eff}^{the} = {} & (0.2 \times \mu_{eff}(\mathrm{Gd})^2 + 0.2 \times \mu_{eff}(\mathrm{Tb})^2 \\ & + 0.2 \times \mu_{eff}(\mathrm{Dy})^2 + 0.2 \times \mu_{eff}(\mathrm{Er})^2 \\ & + 0.2 \times \mu_{eff}(\mathrm{Pr}))^{1/2}\end{aligned} \tag{12}$$

Where μ_{eff}(Gd) = 7.94 μB, μ_{eff}(Tb) = 9.72 μB, μ_{eff}(Dy) = 10.65 μB, μ_{eff}(Er) = 9.58 μB, μ_{eff}(Pr) = 3.58 μB. Hence, the theoretical effective magnetic moment is 8.87 μB, which is consistent with the result obtained from the Curie-Weiss law fit (μ_{eff}^{exp} = 8.45 μB). Furthermore, as the temperature decreases further below TC, the ZFC magnetization increases and eventually saturates, confirming the material exhibits a ferromagnetic state. A marked divergence between the FC and ZFC magnetization curves occurs below TC, with the FC curve being significantly higher. This demonstrates that the spin system freezes into fundamentally different magnetic states depending on whether it is cooled with or without even a small external magnetic field. Below ~100 K, the ZFC magnetization drops sharply, suggesting a possible link to spin freezing.

Figure 5 displays the isothermal magnetization (M-μ₀H) curves of the GdTbDyErPr HEA near the TC under applied magnetic fields up to 5 T. Below the TC, the magnetization increases rapidly in low fields and tends to saturate at higher fields, consistent with typical ferromagnetic behavior., Furthermore, as the temperature higher than TC increases and the magnetic state transitions from a ferromagnetic (FM) to a paramagnetic (PM) state, the M-μ₀H curves progressively approaches a straight line. To understand the nature of the magnetic transition, Belov-Arrott plots are presented in Figure 6. According to the Banerjee criterion, a negative slope in a Belov-Arrott plot indicates a first-order magnetic transition, whereas a positive slope suggests a second-order transition. For a first-order transition, the plot exhibits a pronounced negative slope at temperatures just above the transition point under moderate applied magnetic fields. As the temperature increases, this negative slope shifts to higher field regions and eventually vanishes at the critical endpoint of the transition. In figure 6, obvious negative slope is found and it reveals that the GdTbDyErPr HEA undergoes a first-order magnetic transition near TC.

The isothermal magnetic entropy change ($|\Delta S_M|$) under different magnetic field ranges is determined by integrating the Maxwell relation,

$$\Delta S_M = \int_{H_{min}}^{H_{max}} \left(\frac{\partial M}{\partial T}\right)_H dH \quad (13)$$

Where Hmin and Hmax represent the initial magnetic field and final magnetic field, respectively. Figure 7 shows the calculated ΔS_M-T curves under different magnetic field variations. For a field change of 0 T to 5 T, the peak magnetic entropy change (($\left|\Delta S_M^{pk}\right|$) of the GdTbDyErPr alloy reaches 6.8 J·kg^{-1}·K^{-1} near its TC. This value is considerably higher than that of GdTbErAlFe amorphous alloy (5.9 J·kg^{-1}·K^{-1}) [41], GdHoErAlFe amorphous alloy (5.1 J·kg^{-1}·K^{-1}) [42], GdCoAlY amorphous alloy (5.1 J·kg^{-1}·K^{-1}) [43] and so on under 0-5 T. The refrigerant capacity (RC) and relative cooling power (RCP) are two key parameters for evaluating the heat transfer between the hot and cold reservoirs in an ideal refrigeration cycle,

$$RC = \int_{T_{cold}}^{T_{hot}} |\Delta S_M| \, dT \quad (14)$$

$$RCP = \left|\Delta S_M^{pk}\right| \times \Delta T_{FWHM} \quad (15)$$

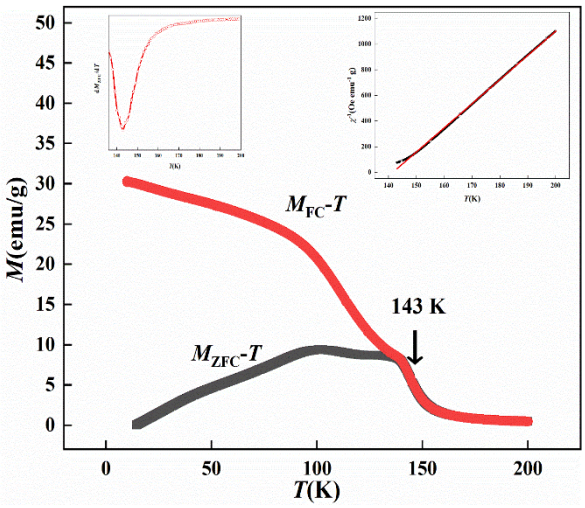

Figure 4. Temperature dependence of M_{FC}-T and M_{ZFC}-T curves for the GdTbDyErPr HEA under an applied magnetic field of 0.05 T. The inset shows dM/dT curve and reciprocal susceptibility (χ^{-1}) as a function of temperature for the GdTbDyErPr HEA.

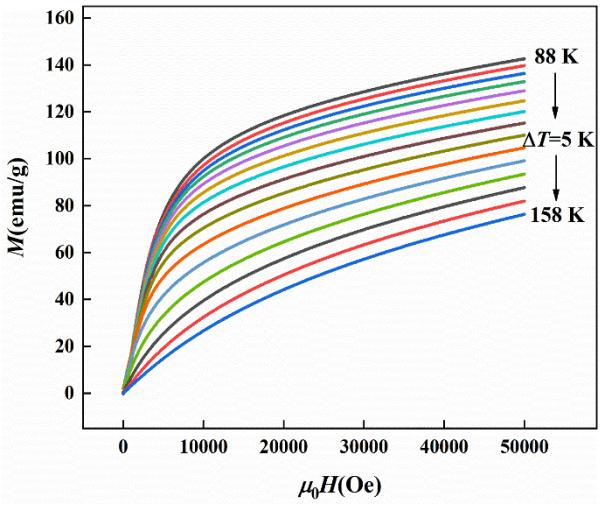

Figure 5. The isothermal magnetization curves for GdTbDyErPr HEA.

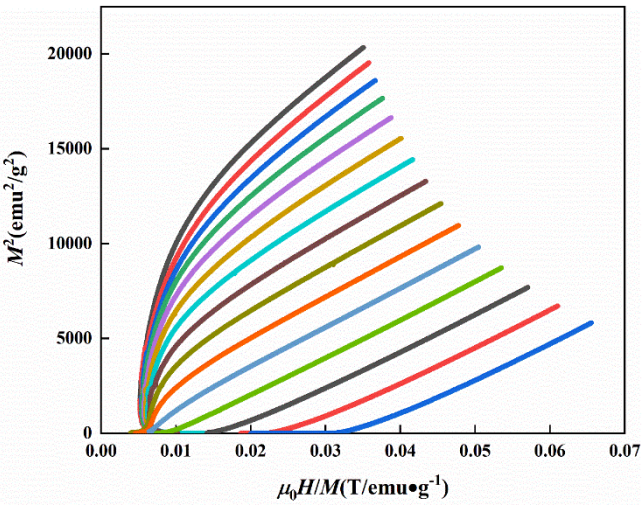

Figure 6 The Arrott plots for GdTbDyErPr HEA.

Table 1 Comparison of magnetocaloric parameters for typical high-entropy alloys.

Sample	Structure	$T_C(T_N)$/K	$\left\|\Delta S_M^{pk}\right\|$/J·kg^{-1} K^{-1}	*RCP*/J·kg^{-1}	$\mu_0 H$/T	Ref.
GdTbDyErPr	Crystal	143	6.8	462	5	This work
GdTbHoErLa	Crystal	127	5.9	391	5	[43]
GdTbHoErY	Crystal	163	5.4	453	5	[43]
GdTbHoErLaY	Crystal	120	5.9	246	5	[43]
GdDyErCoAl	Amorphous	43	9.1	619	5	[35]
TbDyErCoAl	Amorphous	29	8.6	525	5	[35]
TmDyErCoAl	Amorphous	13	11.9	405	5	[35]
TmHoErCoAl	Amorphous	9	15.0	375	5	[44]
Gd25Y15Dy10Co25Al25	Amorphous	44	6.76	424	5	[34]
Gd25Y15Ho10Co25Al25	Amorphous	41	7.35	488	5	[34]
Gd25Y15Er10Co25Al25	Amorphous	43	6.96	477	5	[34]

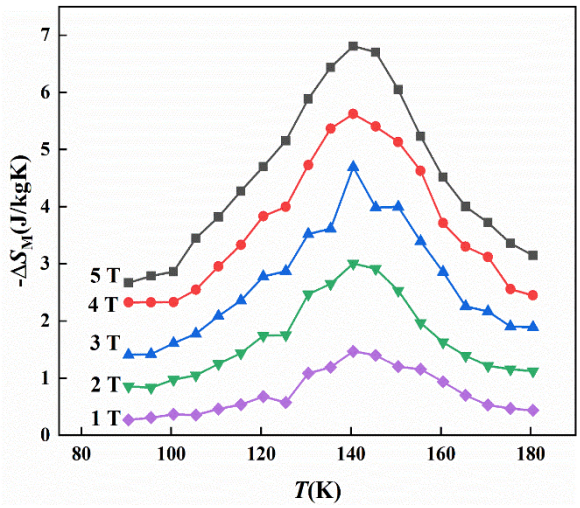

Figure 7. Magnetic entropy change $|\Delta S_M|$ of the GdTbDyErPr HEA as a function of temperature under a maximum applied field of 1 T, 2 T, 3 T, 4 T, and 5 T.

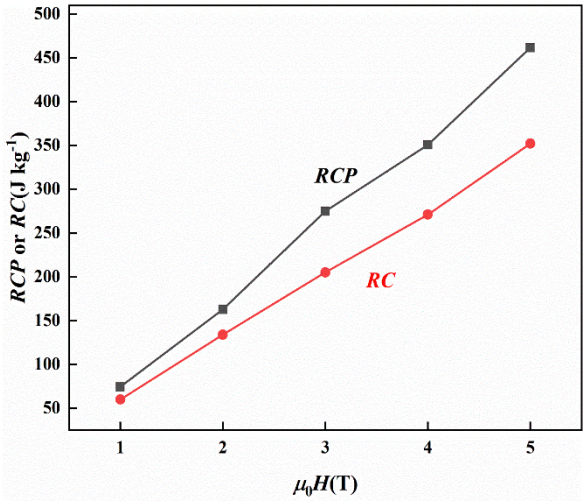

Figure 8. RC and RCP of the GdTbDyErPr HEA as a function of applied field.

Where ΔT_{FWHM} represents the full width at half maximum (FWHM) of the ΔSM-T curves, and $T_{cold(hot)}$ is the temperature at the end of ΔT_{FWHM}. Figure 6 shows the calculated values of RC and RCP as functions of the applied magnetic field. Under a magnetic field change of 5 T, the RC and RCP values for the GdTbDyErPr HEA were determined to be 352 J·kg^{-1} and 462 J·kg^{-1}, respectively. These remarkable refrigerant capacity values originate from the combined effects of a broad refrigeration temperature span and a large magnetic entropy change. Table 1 lists the magnetocaloric parameters of representative crystalline and amorphous high-entropy alloys, which reveals that the phase transition temperature of rare-earth-based high-entropy metallic glasses is typically below 100 K, making them suitable for lower-temperature refrigeration. In comparison, the crystalline GdTbDyErPr high-entropy alloy exhibits magnetocaloric properties comparable to those of other materials.

4. Conclusion

An as-cast GdTbDyErPr rare-earth high-entropy alloy (HEA) was prepared by arc melting, and its structure, magnetic, and magnetocaloric properties were investigated. XRD, SEM, and EDS results confirm that the as-cast GdTbDyErPr RE HEA consists of a single phase with a homogeneous elemental distribution. The chemical composition of this single phase matches the nominal design, and it possesses a hexagonal close-packed (HCP) crystal structure with the space group P63/mmc. The calculated parameter Ω, δ and εi indicates that the GdTbDyErPr RE HEA meets the criteria for forming a homogeneous solid solution. The Curie temperature (TC) was determined to be approximately 143 K using two independent methods: derivative analysis of the MZFC-T curve and Curie-Weiss fitting of its para-magnetic region, with both methods yielding consistent results. Furthermore, the theoretical effective magnetic moment μ_{eff}^{the} is in close agreement with the value μ_{eff}^{exp} obtained from the Curie-Weiss fit, being approximately 8.87 μB. Belov-Arrott plots analysis reveals that the GdTbDyErPr RE HEA undergoes a first-order magnetic transition (FOMT), corresponding to the ferromagnetic-to-paramagnetic transition near TC. The GdTbDyErPr alloy exhibits outstanding magnetocaloric performance. Under a magnetic field change of 0 T to 5 T, it achieves a peak magnetic entropy change ($\left|\Delta S_M^{pk}\right|$) of 6.8 J·kg^{-1}·K^{-1}, a relative cooling power (RCP) of 462 J·kg^{-1}, and a refrigeration capacity (RC) of 352 J·kg^{-1}. These values surpass those of some high-entropy bulk metallic glasses, highlighting its significant potential for magnetic refrigeration applications.

Declaration of competing interest

The authors declare that they have no known competing financial interests or personal relationships that could have appeared to influence the work reported in this paper.

Data availability

Data will be made available on request.

Acknowledgments

This work was supported by Central Government Guidance Funds for Local Science and Technology Development (No.2024ZY0141).

References

[1] A. Czernuszewicz, Y. Mudryk, J. Cui, L. Griffith, D. D. Johnson, and J. Slaughter, "From the discovery of the giant magnetocaloric effect to the development of high-power-density systems," *Advanced Materials Technologies*, vol. 10, no. 5, p. e00545, 2025.

[2] P. Z. Z. Nehan, O. Vitayaya, D. R. Munazat, M. T. E. Manawan, D. Darminto, and B. Kurniawa, "The magnetocaloric effect properties for potential applications of magnetic refrigerator technology: A review," *Physical Chemistry Chemical Physics*, vol. 26, no. 19, p. 14476, 2024.

[3] A. M. Aliev, and A. G. Gamzatov, "Magnetocaloric effect in alternating magnetic fields: a review," *Physics of Metals and Metallography*, vol. 125, no. 12, pp. 1901–1926, 2024.

[4] K. Ahn, "Ni-Mn based conventional full Heusler alloys, all-d-metal full Heusler alloys, and their promising functional properties to solid state cooling by magnetocaloric effect,"*Journal of Alloys and Compounds*, vol. 978, p. 173378, 2024.

[5] F. Q, Zhang, X. F. Miao, N. van Dijk, E. Brück, and Y. Ren, "Advanced magnetocaloric materials for energy conversion: Recent progress, opportunities, and perspective," *Advanced Energy Materials*, vol. 14, no. 28, p. 2400369, 2024.

[6] Y. Gong, X. F. Miao, F. J. Qian, F. Xu, and L. Caron, "A brief review of microstructure design in transition metal-based magnetocaloric materials,"*Journal of Physics: Condensed Matter*, vol. 36, no. 50, p. 503001, 2024.

[7] S. Kumar, R. Muhammad, S. Kim, J. Yi, K. Son, and H. Oh, "Exploring magnetocaloric materials for sustainable refrigeration near hydrogen gas liquefaction temperature," *Advanced Functional Materials*, vol. 34, no. 30, p. 240513, 2024.

[8] A. Vinod, D. A. Babu, and M. Wuppulluri, "A short review on the evolution of magnetocaloric $La(Fe,Si)_{13}$ and its fabrication through melt spinning,"*ACS Omega*, vol. 9, no. 10, pp. 11110–11128, 2024.

[9] L. Cirillo, S. Gargiulo, A. Greco, C. Masselli, V. Orabona, and L. Verneau, "A review of the state of the art of the cryogenic magnetocaloric systems for gas liquefaction," *International Journal of Refrigeration*, vol. 179, pp. 184–203, 2025.

[10] U. Lucia, and G. Grisolia, "Magnetocaloric refrigeration in the context of sustainability: A review of thermodynamic bases, the state of the art, and future prospects," *Energies*, vol. 17, no. 14, p. 3584, 2024.

[11] K. Klinar, J. Y. Law, V. Franco, X. Moya, and A. Kitanovski, "Perspectives and energy applications of magnetocaloric, pyromagnetic, electrocaloric, and pyroelectric materials," *Advanced Energy Materials*, vol. 14, no. 33, p. 2401739, 2024.

[12] Z. Zheng, F. Zhang, H. Shentu, X. Hu, Q. Wu, M. Pan, N. Yu, J. Fang, H. Ge, and H. Yang, "Magnetic properties and magnetocaloric effect of chromium-based high-entropy perovskite oxides," *Journal of Alloys and Compounds*, vol. 1010, p. 177632, 2025.

[13] V. K. Pecharsky, and K. A. Gschneidner, Jr., "Giant magnetocaloric effect in $Gd_5(Si_2Ge_2)$," *Physical Review Letters*, vol. 78, no. 23, pp. 4494-4497, 1997.

[14] J. M. Xu, J. M. Lin, L. Y. Zhu, X. J. Chen, and Y. K. Zhang, "Structural and low-temperature magnetic properties in Ba_2GdBiO_6 double-perovskite oxide," *Solid State Communications*, vol. 411, p. 116359, 2026.

[15] J. M. Lin, X. J. Chen, L. Y. Zhu, K. Zhe, X. Y. Zhao, and Y. K. Zhang, "Cryogenic magnetic properties and magnetocaloric effect in Gd_2YNbO_7 oxide," *Cryogenics*, vol. 156, p. 104313, 2026.

[16] X. P. Na, Y. Z. Du, Z. Q. Zhang, Y. Li, and L. W. Li, "Magnetic properties and magnetocaloric effect in DyAgSi compound," *Cryogenics*, vol. 156, p. 104310, 2026.

[17] Y. Z. Na, W. X. Hao, X. Y. Zhao, Y. Xie, and Y. K. Zhang, "Magnetic properties and cryogenic magnetocaloric effects in $RE_2Zr_2O_7$ (RE = Gd, Dy, Ho and Er) ceramics," *Ceramics International*, vol. 51, no. 20, Part B, pp. 31140–31149, 2025.

[18] N. A. de Oliveira, and P. J. von Ranke, "Theoretical aspects of the magnetocaloric effect," *Physics Reports*, vol. 489, no. 4–5, pp. 89–159, 2010.

[19] V. Franco, J. S. Blázquez, J. J. Ipus, J. Y. Law, L. M. Moreno-Ramírez, and A. Conde, "Magnetocaloric effect: From materials research to refrigeration devices," *Progress in Materials Science*, vol. 93, pp. 112–232, 2018.

[20] A. M. Tishin, and Y. I. Spichkin, "Recent progress in magnetocaloric effect: Mechanisms and potential applications," *International Journal of Refrigeration*, vol. 37, pp. 223–229, 2014.

[21] Y. Wang, H. Pan, and S. Liu, "Research progress of high efficiency magnetic refrigeration technology and magnetic materials," *Journal of Superconductivity and Novel Magnetism*, vol. 38, no. 1, p. 86, 2025.

[22] L. Gao, J. H. Huang, Y. D. Zhang, Y. R. Guo, P. Y. Wang, and Z. Q. Ou, "Research and development of room-temperature magnetic refrigerant and magnetic refrigerator," *Journal of Refrigeration*, vol. 43, no. 4, pp. 77–87, 2022.

[23] J. Liu, T. Gottschall, K. P. Skokov, J. D. Moore, and O. Gutfleisch, "Giant magnetocaloric effect driven by structural transitions," *Nature Materials*, vol. 11, no. 7, pp. 620–626, 2012.

[24] R. Bjørk, C. R. H. Bahl, A. Smith, and N. Pryds, "Review and comparison of magnet designs for magnetic refrigeration,"

International Journal of Refrigeration, vol. 33, no. 3, pp. 437–448, 2010.

[25] M. S. Kamran, H. O. Ahmad, and H. S. Wang, "Review on the developments of active magnetic regenerator refrigerators-evaluated by performance," *Renewable and Sustainable Energy Reviews*, vol. 133, p. 110247, 2020.

[26] P. Sharma, V. K. Dwivedi, and S. P. Dwivedi, "Development of high entropy alloys: a review," *Materials Today: Proceedings*, vol. 43, pp. 502–509, 2021.

[27] Y.-F. Yang, F. Hu, T. Xia, R.-H. Li, J.-Y. Bai, J.-Q. Zhu, J.-Y. Xu, and G.-F. Zhang, "High entropy alloys: A review of preparation techniques, properties and industry application," *Journal of Alloys and Compounds*, vol. 1010, p. 177691, 2025.

[28] M. H. Tsai and J. W. Yeh, "High-entropy alloys: A critical review," *Materials Research Letters*, vol. 2, no. 3, pp. 107–123, 2014.

[29] W. D. Li, D. Xie, D. Y. Li, Y. Zhang, Y. F. Gao, and P. K. Liaw, "Mechanical behavior of high-entropy alloys," *Progress in Materials Science*, vol. 118, p. 100777, 2021.

[30] Z. F. Zhang, L. Chu, J. Q. Zhao, B. Xu, and Q. L. Ye, "Phase separation promotes FCC-phase mechanical twinning in $AlCoCrFeMo_{0.05}Ni_2$ high entropy alloy," *Journal of Metals, Materials and Minerals*, vol. 34, no. 3, p. 2107, 2024.

[31] Y. Qiu, S. Thomas, M. A. Gibson, H. L. Fraser, and N. Birbilis, "Corrosion of high entropy alloys," *npj Materials Degradation*, vol. 1, no. 1, p. 15, 2017.

[32] N. A. Zarkevich and V. I. Zverev, "Viable materials with a giant magnetocaloric effect," *Crystals*, vol. 10, no. 9, p. 815, 2020.

[33] L. Shao, L. Xue, Q. Luo, K. Yin, Z. Yuan, M. Zhu, T. Liang, Q. Zeng, L. Sun, and B. Shen, "Heterogeneous GdTbDyCoAl high-entropy alloy with distinctive magnetocaloric effect induced by hydrogenation," *Journal of Materials Science & Technology*, vol. 109, pp. 147–156, 2022.

[34] C. M. Pang, L. Chen, H. Xu, W. Guo, Z. W. Lv, J. T. Huo, M. J. Cai, B. L. Shen, X. L. Wang, and C. C. Yuan, "Effect of Dy, Ho, and Er substitution on the magnetocaloric properties of Gd-Co-Al-Y high entropy bulk metallic glasses," *Journal of Alloys and Compounds*, vol. 827, p. 154101, 2020.

[35] J. Li, L. Xue, W. M. Yang, C. C. Yuan, J. T. Huo, and B. L. Shen, "Distinct spin glass behavior and excellent magnetocaloric effect in $Er_{20}Dy_{20}Co_{20}Al_{20}RE_{20}$ (RE = Gd, Tb and Tm) high-entropy bulk metallic glasses," *Intermetallics*, vol. 96, pp. 90–93, 2018.

[36] X. Yang, and Y. Zhang, "Prediction of high-entropy stabilized solid-solution in multi-component alloys," *Materials Chemistry and Physics*, vol. 132, no. 2–3, pp. 233–238, 2012.

[37] B. Miracle, J. D. Miller, O. N. Senkov, C. Woodward, M. D. Uchic, and J. Tiley, "Exploration and development of high entropy alloys for structural applications," *Entropy*, vol. 16, no. 1, pp. 494-525, 2014.

[38] S. S. Fang, X. S. Xiao, L. Xia, W. H. Li, and Y. D. Dong, "Relationship between the widths of supercooled liquid regions and bond parameters of Mg-based bulk metallic glasses," *Journal of Non-Crystalline Solids*, vol. 321, no. 1–2, pp. 120–125, 2003.

[39] S. Guo, C. Ng, J. Lu, and C. T. Liu, "Effect of valence electron concentration on stability of fcc or bcc phase in high entropy alloys," *Journal of Applied Physics*, vol. 109, no. 10, p. 103505, 2011.

[40] S. Guo, and C. T. Liu, "Phase stability in high entropy alloys: Formation of solid-solution phase or amorphous phase," *Journal of Non-Crystalline Solids*, vol. 321, no. 1–2, pp. 120–125, 2003.

[41] H. J. Ma, L. Gao, X. Jin, J. J. Zhao, J. Zhao, and J. H. Huang, "Low-temperature magnetic refrigeration in $Gd_{20}Tb_{20}Er_{20}Al_{20}M_{20}$ (M = Fe, Co) high-entropy metallic glasses," *Chinese Journal of Physics*, vol. 92, pp. 353–365, 2024.

[42] W. Sheng, J. Q. Wang, G. Wang, J. T. Huo, X. M. Wang, and R.-W. Li, "Amorphous microwires of high entropy alloys with large magnetocaloric effect," *Intermetallics*, vol. 96, pp. 79–83, 2018.

[43] S. F. Lu, L. Ma, J. Wang, Y. S. Du, L. Li, J. T. Zhao, and G. H. Rao, "Effect of configuration entropy on magnetocaloric effect of rare earth," *Journal of Alloys and Compounds*, vol. 874, p. 159981, 2021.

[44] J. T. Huo, L. Huo, J. Li, H. Men, X. Wang, A. Inoue, C. Chang, J.-Q. Wang, and R.-W. Li, "High-entropy bulk metallic glasses as promising magnetic refrigerants," *Journal of Applied Physics*, vol.117, p. 073902, 2015.